Sparse innervation and local heterogeneity in the vibrissal corticostriatal projection

Abbreviated title : Functional somatosensory corticostriatal connectivity

Authors and affiliations:

Kenza Amroune[1], Lorenzo Fontolan[2], Agnès Baude[1], David Robbe[2] and Ingrid Bureau[1]*

[1] Aix-Marseille Université, INSERM, INMED, Marseille, 13009, France

[2] Aix-Marseille Université, INSERM, INMED, Turing Centre for Living Systems, Marseille, 13009, France

corresponding author email address: ingrid.bureau@inserm.fr

Abstract

The density and overlap of cortical axons in the dorsolateral striatum (DLS) have suggested that striatal neurons integrate widespread information from cortical regions that are functionally related. However, in vivo, DLS neuronal responses to sensory stimuli have shown unexpectedly high selectivity, raising questions about the actual degree of input convergence of functional corticostriatal projection on individual striatal cells. Here, we investigated this question by focusing on the projections from different whisker cortical columns, as they overlap in the striatum and are co-active during behavior. Using *ex vivo* patch-clamp recordings in the DLS and glutamate uncaging for focal stimulations in the barrel cortex, we were able to map the location of presynaptic neurons to individual striatal projection neurons (SPNs). We found that each SPN was innervated by cells located in a small number of whisker cortical columns scattered across the barrel field in the slice. Connectivity of single SPNs with cortical neurons was thus highly discontinuous horizontally, despite the presence of more potential connections. Moreover, connectivity patterns were specific to each cell, with neighboring SPNs sharing few common clusters of presynaptic cells in the cortex. Despite this sparse and distinct innervation of individual SPNs, the projection was topographically organized at the population level. Finally, we found similar innervation patterns for D1 and D2-type SPNs, but observed distinct differences in synaptic strength at connections with specific cortical layers, notably with the associative layer 2/3. Our results suggest that the high convergence of somatosensory inputs to the striatum, enabled by diffuse and overlapping cortical innervation, is accomplished through sparse yet complementary connectivity to individual SPNs.

Introduction

The dorsolateral striatum receives dense glutamatergic innervation from all sensory cortical areas. Its presumed function is to monitor the animal's ongoing sensory information, contributing to the modulation of sensory-guided behaviors and the learning of voluntary tasks (Pennartz et al., 2009; Znamenskiy and Zador, 2013; Sippy et al., 20158). The observations that cortical neurons are overabundant compared to striatal projection neurons (SPN) (Oorschot 1996), that axonal projections originating from functionally linked cortical regions overlap in the striatum (Flaherty and Graybiel, 1991; Alloway et al., 1999; Wright et al., 1999; Hooks et al., 2018) and that synaptic glutamatergic inputs must overcome strong feedforward inhibition (Mallet et al., 2005; Pidoux et al., 2011), have led to the idea that striatal neurons integrate dense and broad cortical inputs. In fact, studies examining the density of axonal boutons relative to the single cell dendritic spines have predicted that several thousand cortical neurons could potentially connect every SPN if synapses were formed promiscuously (Kincaid et al., 1998). However if synapses were formed in a selective manner, this would reduce the degree of convergence of cortical input onto individual SPNs and potentially increase the heterogeneity of inputs between SPNs (Kincaid et al., 1998), a scenario with important implications for how cortical information is integrated in the striatum. These alternative connectivity models schematized in Fig. 1 remained to be tested functionally.

Here, we investigated this question at the level of the projections to SPNs originating from the barrel field in the mouse primary somatosensory cortex (S1). Vibrissal information is transmitted to the cortical columns of S1 through parallel sensory channels, each corresponding to an individual whisker (reviewed in Adibi 2019). In S1, layer 4 contains optically dense, barrel-shaped structures whose organization mirrors the spatial arrangement of whiskers on the snout. This feature provides a framework for studying neuronal connectivity in relation to the whisker cortical columns *ex vivo*. However, this model has not yet been used to examine connectivity within the functional vibrissal corticostriatal projections, leaving the degree of input convergence in this pathway unclear. On the one hand, axons of neurons located in different whisker cortical columns overlap heavily in the dorsal striatum, suggesting that SPNs could receive dense and broad vibrissal cortical input (Wright et al., 1999; Alloway et al., 2000). On the other hand, cell activity evoked by whisker deflection showed notable heterogeneity in the DLS: neurons were either tuned to multiple whiskers, selective to a single whisker, or yet non-responsive (Carelli and West, 1991; Pidoux et al., 2011). These observations prompted us to investigate whether the vibrissal

innervation of SPNs violated Peters' rule stating that connectivity is proportional to the overlap of axons and dendrites (Peters, 1979; Braitenberg and Schüz, 1998).

SPNs comprise two distinct populations, defined by their projection targets and expression of dopamine receptors: D1 receptors in the direct pathway and D2 receptors in the indirect pathway (Smith et al., 1998; Kravitz et al., 2010) (neurons are hereafter referred to as D1 and D2 SPNs). Studies have found that inputs received by D1 SPNs were stronger than those received by D2 SPNs (Kress et al., 2013; Reig and Silberberg, 2014; Parker et al., 2016; Filipović et al., 2019). These observations may indicate that inputs converge to different degrees to D1 and to D2 SPNs.

To investigate the connectivity and input convergence on SPNs, we used a functional mapping technique that combines patch-clamp recordings and laser scanning photostimulation (LSPS) with glutamate uncaging on a novel slice preparation, which preserved the organization of the vibrissal corticostriatal projections, from the superficial layers of the barrel cortex to the DLS. The sites in the barrel cortex where LSPS evoked synaptic currents indicated the location of neuronal somas that were presynaptic to the recorded SPN. We found overall discrete innervations, as presynaptic neurons were thinly-scattered across the barrel field, or present in a single cortical column. SPNs located nearby in the same slice had distinct patterns of innervation, suggesting that connections on each SPN were fewer than the local potential connections. No difference was found between the innervation patterns of D1 and D2 SPNs, but the strength of their connections with certain layers differed.

Results

A novel preparation for investigating functionally the organization of projections from the barrel cortex to individual SPNs in the DLS

To investigate the spatial organization of sensory projections to SPNs, we have developed a parasagittal somatosensory corticostriatal slice, which visibly contained ~ 8 whisker barrels (Methods; Fig. 2A and Supplemental Fig. 1A). Biocytin-labeled projections extended from the top of the barrel cortex to the DLS (Fig. 2A,B). To further validate the angles used in the preparation, we virtually re-sectioned a brain from the Allen Mouse Connectivity Atlas in which pyramidal cells of the barrel cortex had been labeled *in vivo* (i.e., prior to slicing; Supplemental Fig. 1B). Cortical axons extended into the striatum in a similar manner in both the reconstituted and acute slices (compare Fig. 2A and Supplemental Fig. 1B), supporting the idea that projections from the present cortical columns targeting the recorded striatal region were largely preserved in the acute slice. Animals were Drd1a-tdTomato hemizygous mice in

88 which D1 receptor expressing neurons were labeled. $D1^+$ and $D1^-$ ($D2^+$) SPNs were recorded in the
89 whole-cell voltage–clamp configuration (n = 101 cells, N = 54 mice). Simultaneously, an ultraviolet laser
90 beam was directed at every site of a 29 x 16 pixel grid (2.1 × 1.1 mm, 75 µm spacing) to uncage
91 glutamate over the barrel cortex, excite cortical neurons, and thereby reveal cells presynaptic to the
92 recorded SPN (Fig. 2C,D). When glutamate was uncaged on an excitatory cortical neuron innervating the
93 recorded SPN, it elicited short-lived excitatory postsynaptic currents (EPSCs; < 50 ms duration) (Fig. 2D).
94 We and others have shown that only subthreshold synaptic events are elicited with this method,
95 implying that the evoked EPSCs are mono-synaptic and that feedforward inhibition is prevented
96 (Shepherd et al., 2003; Bureau et al., 2008). In fact, glutamate uncaging excited cortical neurons above
97 their firing threshold at a maximal distance of 75 µm from their cell body (Fig. 1E; Supplemental Fig. 2A),
98 on 2.8 ± 0.3 sites of the LSPS grid (mean ± sem; L5 pyramidal cells, n = 40; 75 µm spacing grid; see
99 Methods), consistent with a direct (i.e., non synaptic) and nearly somatic excitation (data per cell type in
100 the Methods and Supplemental Fig. 2). Thus, the sites where LSPS evoked EPSCs in SPNs contained or
101 were adjacent to the cell bodies of cortical neurons that were directly connected to the recorded cell.
102 These sites are hereafter referred to as "connected sites". EPSCs had small amplitudes, 40 ± 1 pA (n =
103 550), consistent with the presence of only one or a few presynaptic cells (≤ 5) at each connected site of
104 the map.

105 For each SPN, an input map was assembled from the excitatory response evoked at the uncaging sites of
106 the LSPS grid (Fig. 2D, top). From this input map, a binary map was derived which reported the presence
107 or lack of evoked EPSC, referred to as "connectivity map". We first analyzed the ensemble of
108 connectivity maps to characterize the global organization of the projections from the barrel field in the
109 slice and checked that their properties were consistent with those described by anatomical studies (Fig.
110 2F). When all SPN connectivity maps were superimposed and overlaid on the barrel cortex (see
111 Methods; Fig. 2F), the connected sites principally highlighted the layer (L) 5a. Indeed, ~ 65 % of all SPNs
112 received input from this layer (Fig. 2G). Responses were elicited less frequently when stimulations were
113 in L4, L5b, L2/3 and in L6. We found that 50 % of L5a cells fired action potentials when stimulations were
114 at the bottom of L4, indicating that a fraction of the relatively high connectivity rate seen at the bottom
115 of L4 was in fact with nearby L5a pyramidal cells (Fig. 2E; Supplemental Fig. 2A). In contrast, photo-
116 stimulations in L2/3 never elicited the firing of L5a cells (n = 11; Fig. 2E), indicating that all EPSCs evoked
117 by stimulations in these superficial layers arose from direct synaptic connections between L2/3
118 pyramidal cells and SPNs. EPSCs evoked with stimulations in L2/3 to L5b had similar amplitudes (Fig. 2H),

suggesting that L5a dominated these other layers thanks to a greater connectivity with SPNs principally. However, L6-EPSCs were smaller compared to L5a and L5b-EPSCs (Kruskal-Wallis, H(4) = 22.8, p = 0.0001; Dunn post-hoc test and Šidák correction, p = 0.0001 and 0.034; Fig. 2H). These observations are aligned with the anatomical studies which have identified L5a as the primary, although not exclusive, source of cortical innervation in the DLS (Wise and Jones, 1977; Cowan and Wilson, 1994; Wall et al., 2013).

In the superimposed connectivity maps, the ensemble of connected sites observed across recordings formed a band in the barrel cortex that was larger than the region in the DLS containing the recorded SPNs (2.5 mm vs. 1 mm, Fig. 2F). An opposite asymmetry was observed when analyzing the striatal region connected to individual cortical columns: sites within a single cortical column (~ 150 µm in this preparation) were connected to SPNs distributed across a larger striatal region, spanning about 600 µm (Fig. 2I). These two asymmetric relationships (converging vs. diverging), summarized in Fig. 2J, implied that functional projections from adjacent cortical columns overlapped in the DLS, which is consistent with their known anatomy (Wright et al., 1999; Alloway et al., 2000; Hooks et al., 2018). Thus, projections from the cortical columns in the slice overlapped in the striatum, which allowed us to investigate the degree of convergence of whisker cortical inputs onto individual SPNs.

Low convergence of projections from the barrel cortex to individual SPNs in the DLS

To investigate the number and position of whisker cortical columns from which individual SPNs received synaptic inputs, each connectivity map was collapsed along its vertical axis and the horizontal distribution of connected sites was characterized using the following metrics (Fig. 3A): 1- the input field, or the overall region within the barrel field in the slice from which an SPN receives inputs. Its width is the distance between the SPN most distant connected sites.; 2- the cluster, a region in the collapsed connectivity map constituted of adjacent connected sites; 3- the cortical column, or its proxy: 1 to 2 adjacent connected sites in the collapsed connectivity map (i.e. 75-150 µm width). The connected sites were organized in 1 to 6 clusters, 1.9 ± 0.1 on average in the input fields (Fig. 3B). Typically, the width of clusters was about one cortical column (171 ± 7 µm) and it rarely exceeded two adjacent columns (Fig. 3C). Finally, SPNs were innervated by cells distributed in close to 3 columns (2.7 ± 0.2), though some SPNs with several clusters (54 %) were innervated by as many as eight columns (Fig. 3D). The distance between clusters was 75 to 900 µm, 265 ± 28 µm on average (n = 55; Fig. 3C). Thus, SPNs could receive inputs from clusters of cortical cells separated by substantial connectivity gaps, often spanning several columns. Heterogeneous spacing and number of clusters contributed to the variability of the input fields

150 width, which ranged between 0.075 and 1.6 mm (average, 535 ± 42 µm; Fig. 3E). Strikingly, 45 % of the
151 input fields with several clusters produced no synaptic response upon stimulation (map collapsed along
152 the vertical axis; Fig. 3F, bottom). Moreover, the number of clusters was not increased proportionally in
153 very large input fields, > 1.4 mm, in which connectivity gaps amounted to more than 50 % of space in
154 the horizontal axis (Fig. 3F, bottom). Altogether, these findings suggest a connectivity pattern
155 characterized by a few small patches of presynaptic cortical cells scattered across the axis of barrels.

156 It could be that small input fields that contained a single cortical column (75-150 µm) were obtained
157 when recordings were performed on the edges of the striatal region with cortical innervation in the
158 slice. Contrary to this hypothesis, we found that SPNs with small input fields and those with broader
159 ones were intermingled along the horizontal axis in the striatum (open and solid symbols in Fig. 3G,
160 respectively). In fact, the width of the input fields remained relatively constant across SPN positions in
161 the slice (Fig. 3G, top; Spearman correlation coefficient, R = 0.05, p = 0.61). This suggests that the
162 position of our recordings did not impact the SPN input fields. Furthermore, SPNs receiving input from a
163 single column were often located near others receiving input from multiple ones (Fig. 3D), reinforcing
164 that the low functional connectivity with barrel columns in the slice was genuine in these cases.

165 Next, we investigated these connectivity patterns along their vertical axis. Individual SPNs had
166 connected sites distributed in 2.4 ± 0.1 cortical layers on average (2.9 ± 0.1 for SPNs with several
167 clusters). But these sites were not necessarily vertically aligned within a cortical column (examples in Fig.
168 2D and 3A). In fact, in 55 % of the cases, a column of the barrel field innervated an SPN through
169 projections from a single cortical layer. This suggests that neurons projecting to an SPN are dispersed in
170 the barrel cortex in such a way that the transmitted inputs may originate from distinct layers as well as
171 from different whisker cortical columns. Our findings are summarized in Fig. 3H, with schematics of the
172 average and principal connectivity patterns.

173 **Individual SPNs have unique innervation**

174 The above analysis has revealed great heterogeneity between SPN innervations. We then investigated
175 whether innervations were more similar when SPNs were close to each other. To address this question,
176 we compared the connectivity patterns of SPNs recorded in the same slice (Fig. 4A). First, we observed
177 that the majority of SPN pairs had their input fields overlapping in the barrel cortex (n = 70; Fig. 4B). The
178 ratio was the highest, 77 %, for SPNs that were neighbors in the striatum (< 100 µm, n = 33), but
179 remained above 50 % for cell distances of 400-500 µm. We next examined to what extent the connected

180 sites were shared or vertically aligned between the connectivity maps. In contrast to input fields,
181 alignment or overlap of connected sites was only observed when SPNs were less than 300 µm apart (Fig.
182 4B,C). Moreover, this concerned only a small fraction of the pair's connected sites: when SPNs were less
183 than 100 µm apart, only 18 ± 2 % of the connected sites in the two connectivity maps were vertically
184 aligned and 7.7 ± 1.6 % of them overlapped (Fig. 4B,C). Overall, these results indicate that DLS SPNs
185 could receive inputs from the same domain in the barrel cortex and yet have patterns of cortical
186 innervation without or little redundancy. They support a connectivity model in which synaptic
187 connections on each SPNs are sparser than the potential connections, and with significant heterogeneity
188 between SPNs in terms of their whisker-related cortical inputs.

189 **Topographic organization of SPN functional vibrissal innervation**

190 The sparse innervation patterns with little similarities of neighboring SPNs might be inconsistent with a
191 topographic organization. To examine the global organization of functional projections, connectivity
192 maps of SPNs were superimposed, and the connected sites were labeled based on the SPN positions in
193 the striatum (Fig. 5A). SPNs located laterally/medially in the dorsal striatum had an input field whose
194 connectivity center of mass (CM, see Methods) was in the lateral/medial part of the barrel cortex (Fig.
195 5A,B). Thus, the functional projections from the barrel cortex were topographically organized in the DLS,
196 consistent with anatomy (Flaherty and Graybiel, 1991; Alloway et al., 1999; Wright et al., 1999; Hooks et
197 al., 2018). Given the orientation of the slice (Supplemental Fig. 1A), a shift of the connectivity CM on the
198 horizontal axis of the barrel field corresponded principally to a shift between whisker arcs (e.g. E1 to E8
199 barrel). The connectivity CMs of two adjacent SPNs could be 1 mm apart in the barrel cortex (Fig. 5B),
200 indicating that the topographic organization was not as precise as for intracortical projections (Shepherd
201 and Svoboda, 2005; Erlandson et al., 2015). This finding, together with previous analyses, supports a
202 connectivity model that falls between the two illustrated in the middle and right panels of Fig. 1
203 (selective, broad and loosely topographic)

204 EPSC amplitudes were heterogeneous within each input map (Fig. 5C; ex Fig. 2D). To test the hypothesis
205 of a topographic organization influencing synaptic strength, we examined whether strong connections
206 were associated with presynaptic cells located close to the connectivity CM. If such an organization of
207 synaptic strengths existed, we would expect it to improve the correlation between the CM of synaptic
208 input maps and SPN positions. However, we found nearly identical correlations whether taking the
209 connectivity CM or the synaptic input CM, which is based on the connectivity pattern weighted by EPSC
210 amplitudes (see Methods; R = 0.60 vs. 0.62; F(1) = 115.08, p = 0.98, ANCOVA; Fig. 5D). While residuals

211 from the correlation curve tended to be smaller using synaptic input CMs, the difference was not
212 statistically significant (- 9 ± 7 µm, p = 0.084, Wilcoxon, SPNs with >1 cluster). This was because synaptic
213 input CMs were only slightly shifted from the connectivity CMs, by 45 ± 5 µm for SPNs with two or more
214 clusters (Fig. 5D). These findings indicate that EPSC amplitudes showed no consistent pattern relative to
215 the connectivity CM of the input field. This confirms the connectivity patterns as principal determinants
216 of the topographic organization of somatosensory corticostriatal projections.

217 Finally, given that previous studies have revealed that responses of some striatal neurons exhibited
218 strong selectivity for specific whiskers *in vivo* (Carelli and West, 1991; Pidoux et al., 2011), we
219 investigated whether, in cases where SPNs were innervated by multiple clusters, one cluster might
220 dominate the others. Comparing the sum of EPSCs corresponding to clusters, we found substantial
221 variability, with the strongest cluster providing input that was 1.12 to 55 times greater than other
222 clusters within the input field (× 6.8 ± 1.4 on average; Fig. 5E). Thus, connectivity patterns with multiple
223 clusters may still permit some SPNs to have a preference for a particular whisker cortical column, due to
224 the heterogeneity between clusters.

225 **D1 and D2 SPNs receive similar input from the barrel cortex**

226 Finally, we investigated whether innervation patterns differed between the two populations of SPNs,
227 expressing D1 or D2 receptors. Based on previous studies, unlabeled neurons in Drd1a-tdTomato
228 hemizygous mice were principally SPNs expressing the D2 receptor (Bertran-Gonzalez et al., 2008; Ade
229 et al., 2011; Enoksson et al., 2012; Thibault et al., 2013; Cao et al., 2018). As previously reported (Wall et
230 al., 2013), projections to D1 and D2 SPNs were spatially intermingled along the axis of barrels (Fig. 6A,B ;
231 n = 47 and 54, cells respectively). We found that D1 and D2 SPNs had similar input fields: first, their
232 widths were not different (Fig. 6C). In addition, they received input from a similar number of cortical
233 columns, which were organized in clusters of similar widths (Fig. 6D,E). Paired analysis of D1 and D2
234 SPNs recorded in the same slice also showed that their input fields did not significantly differ in width,
235 number of cortical columns or cluster width (p = 0.44 – 0.50 – 0.26, Wilcoxon; Fig. 6C-E). None of these
236 parameters exhibited a clear relationship between subtypes (R = 0.13 – 0.30 – -0.003; p = 0.43 – 0.058 –
237 0.99, Pearson; Fig. 6C-E). Finally, both types of SPNs received input from each cortical layer in similar
238 proportions (Fig. 6F). Thus, the heterogeneity in patterns of innervation is not due to a difference
239 between SPN subtypes. Overall, there was no difference in the total inputs received by D1 and D2 SPNs
240 (EPSC sum or $EPSC^T$; Fig. 6G). In addition, the principal cluster was similarly dominant over the other
241 clusters (Fig. 6H). However, differences were observed in a layer-specific manner (Fig. 6I). Whereas L5-

242 $EPSC^T$ was similar in D1 and D2 cells, differences were found in L2/3 and L6: L2/3-$EPSC^T$ was larger in D2
243 SPNs (132 ± 36 vs. 53 ± 22 pA, p = 0.005, Mann-Whitney) but L6-$EPSC^T$ was larger in D1 SPNs (37 ± 10 vs.
244 16 ± 2 pA, p = 0.038). Further analysis suggested a difference in the strength of synapses as principal
245 mechanism. Indeed, L2/3-EPSCs evoked at single sites were larger in D2 SPNs (48 ± 11 pA vs. 27 ± 5 pA;
246 p = 0.043) whereas L6-EPSCs were larger in D1 SPNs (24 ± 2 pA vs. 16 ± 2 pA ; p = 0.038).

247 ## Discussion

248 We investigated the organization of functional projections originating in the barrel cortex and targeting
249 projection neurons in the dorsal striatum in a novel preparation. We found overall little input
250 convergence as cortical neurons innervating an SPN were either located in a single cortical column or
251 thinly scattered across the barrel field. Each SPN had a distinct pattern of innervation from the barrel
252 cortex, albeit with occasional overlap for SPNs closely positioned in the DLS. D1 and D2 presented
253 similar patterns of innervations.

254 **Sparse sensory innervation of single SPNs**

255 As previously revealed by tracings of corticostriatal projections, the primary source of innervation of
256 SPNs in this study is the upper part of L5 in the barrel cortex, L5a, although, SPNs are occasionally
257 innervated by cells located in deeper and superficial layers (Wise and Jones, 1977; Reiner et al., 2003;
258 Wall et al., 2013; Guo et al., 2017; Yamashita et al., 2018; Bertero et al., 2022). Given the abundance of
259 cortical axons in the striatum, it has been assumed that a large number of cortical cells innervate each
260 SPN, potentially up to few thousands if synaptic connections were made promiscuously (Kincaid et al.,
261 1998). On the other hand, it has also been reported that neurons in the DLS fire in response to the
262 stimulation of a single body-part in monkeys and rodents *in vivo*, even of a single whisker in some cases
263 (Carelli and West, 1991; Jaeger et al., 1995; Cho and West, 1997). This finding suggested that each
264 striatal neuron was in fact innervated by one small subregion of S1, although feedforward inhibition
265 could have masked a broader selectivity (Pidoux et al., 2011). Here, the LSPS connectivity maps indicate
266 that convergence from the barrel cortex to individual SPNs is indeed low as 60 % of SPNs responded to
267 the stimulation of only one or two whisker cortical columns present in the preparation. The LSPS
268 combined with glutamate uncaging maps projections from neuronal cell bodies within the slice.
269 Therefore, our study characterized connectivity patterns rather than the full extent of connectivity with
270 the barrel cortex, as projections from columns outside the slice were not activated. A number of critical
271 findings argue that innervation on individual SPNs is genuinely sparse: i) The cortical columns present in

272 the slice corresponded to different whisker arcs, an axis associated with the greatest overlap of cortical
273 axons in the striatum (Alloway et al., 1999), and therefore where input convergence could have been
274 high. This organization was visible in the global SPN LSPS connectivity map (Fig. 2J). ii) The peak of
275 connectivity was with L5a as previously documented, not with a layer closer to striatum, as this would
276 be the case if the native organization of the projection was altered in the preparation. iii) The connected
277 sites were scattered along broad horizontal and vertical axes, implying that projections in between were
278 preserved. Critically, the fact that adjacent SPNs had different connectivity patterns in the same slice
279 further supported the presence of a pool of potential connections larger than the number of actual
280 connections made on each SPN. iv) Connectivity clusters were sparser in larger input fields, suggesting
281 that the number of presynaptic cells to an SPN was regulated and reached a plateau. v) EPSCs were
282 small, consistent with one or a few presynaptic cells at each connected site. Altogether, our results
283 support the model in which, within a loosely topographical organization of projections, each SPN
284 integrates limited and heterogeneous rather than exhaustive inputs transmitted by the barrel cortex
285 (Fig. 7). The speckled connectivity pattern of individual SPNs, arising from the abundant and diffuse
286 cortical innervation in the DLS, suggests that sensory corticostriatal synapses are established through a
287 selective and/or competitive process.

288 **Specific cortical input to individual SPNs**

289 A peculiar feature of the corticostriatal innervation is the imbalance between the number of cortical
290 cells projecting to the striatum and the number of striatal cells, thought to be at a ratio of 10 to 1
291 (Oorschot, 1996). Based on this ratio and the ultrastructure of the corticostriatal connection, the density
292 of axonal boutons and spines, C. Wilson's group concluded that the probability of an SPN being
293 contacted by one given axon entering the domain of its dendritic arborization was low, 0.04 - 1.4 %,
294 depending on the model. Hence, the chance that two SPNs were innervated by the same cortical axon
295 was even lower according to this model. Consistent with this, here, we found that overlaps between the
296 connectivity maps of SPNs were rare. This indicates that SPNs primarily integrate distinct inputs
297 originating from the barrel cortex. When overlaps were observed, they occurred only for SPNs located
298 within 250 µm of each other. However, such overlaps involved only a small fraction of their inputs, as
299 the connectivity patterns of nearby SPNs were largely interdigitated. In addition, the input fields
300 continued to intersect significantly beyond 250 µm and up to 500 µm of separation between SPNs. This
301 means that relatively distant SPNs can share a general region of connectivity in the barrel cortex without
302 any of their presynaptic partners residing within the same cortical column. Interestingly, the observation

303 that two SPNs must be less than 250 µm apart to share some of their inputs was not predicted by the
304 known ultrastructure of corticostriatal connections. In fact, it predicted the opposite: that two SPNs
305 would more likely to be innervated by the same cortical cell if their dendrites extended into different
306 striatal subregions, as this would increase the likelihood of each SPN contacting boutons of this cortical
307 cell, as these are sparsely distributed in the striatum (Kincaid et al., 1998). One possible explanation for
308 this discrepancy could be that, in our experiments, pairs of SPNs with shared connectivity were
309 innervated by different neurons that were co-localized in the barrel cortex (< 75 µm apart). Such events
310 could also be at the origin of the striatal clusters described *in vivo,* in which neurons had similar, yet non-
311 identical, sensory selectivity (Carelli and West, 1991; Jaeger et al., 1995).

312 **Similarities and specificities in the patterns of projection to SPNs of the direct and indirect pathways**

313 Electrophysiological studies have shown that D1 SPNs exhibit larger responses than D2 SPNs to whisker
314 deflections (Reig and Silberberg, 2014; Filipović et al., 2019). Also, the optostimulation of cortical
315 efferents in brain slices showed a bias towards D1 SPNs (Kress et al., 2013; Parker et al., 2016). In our
316 study, we had contrasting results. There was no difference in the innervation of D1 and D2 SPNs, neither
317 in the rate at which cells were connected by layers, nor in the organization of the projection. The
318 principal layer innervating SPNs, L5a, delivered inputs of similar strengths to D1 and D2 SPNs. However,
319 layers with lower incidence in the pattern of innervation showed bias in the amplitude of responses:
320 stimulations in L2/3 induced stronger responses in D2 cells whereas stimulations in L6 activated D1 cells
321 more strongly. We have shown that stimulation in L2/3 activates the L2/3 projection only. Similarly, the
322 L6-evoked EPSCs are consistent with the axon collaterals that L6 corticofugal projection neurons have in
323 the striatum (Guo et al., 2017; Bertero et al., 2022). The larger L2/3 inputs received by the D2 SPNs is
324 intriguing because of the role of this layer in higher-order integration processes, such as those activated
325 during operant sensory discrimination tasks (Kwon et al., 2016; Han and Helmchen, 2024; Oryshchuk et
326 al., 2024). Moreover, the activity of L2/3 cells during mouse displacement is distinctive, exhibiting a
327 sustained response to ongoing whisker-wall contacts, as opposed to the transient response observed in
328 L5 (Ayaz et al., 2019). In L6, the population of corticofugal projection neurons is diverse, with some
329 responding to whisking and sensory stimuli, while others are active during transitions into quiet periods
330 of behavior (Dash et al., 2022; Vélez-Fort et al., 2014). Further investigation is needed to specifically
331 examine projections from the upper and lower cortical layers and how they influence the dynamics of
332 sensory integration in the direct and indirect pathways of the DLS. However, these data illustrate the
333 diversity of paths of sensory integration involving D1 and D2 SPNs.

334 In conclusion, we found a low and sparse connectivity within the cortical vibrissal projections to
335 individual SPNs. While projections respected a loose topography, the innervation patterns of individual
336 SPNs displayed substantial connectivity gaps and heterogeneity. Since the inputs of each SPN represent
337 only a limited subset of whisker columns, sensory integration must occur at the population level, with
338 each SPN representation complementing the representations of its neighbors (Fig. 7). These
339 observations raise the hypothesis of a selective or competitive process underlying the formation of
340 corticostriatal synapses.

341 Materials and Methods

342 **Animals and ethics**

343 Hemizygous male and female B6.Cg-Tg(Drd1a-tdTomato)6Calak/J mice (JAX stock #016204; Ade et al.,
344 2011) were used on postnatal day 22-43, in accordance with institutional guidelines and the French
345 Ministry of Research (APAFIS#27242).

346 **Brain slices preparation and electrophysiology.**

347 Mice were deeply anesthetized with isoflurane (4 %) prior to cervical dislocation and decapitation. We
348 prepared corticostriatal slices (350 µm thick) from the brain left hemisphere, based on stereotaxic
349 coordinates placing the striatal cells 1-2 mm anteriorly to the projection neurons in the barrel cortex
350 (Aronoff et al., 2010; de la Torre-Martinez et al., 2023). Parasagittal slices were cut with a 60° angle from
351 the midline and a 10° angle in the dorso-ventral axis (Supplemental Fig. 1A) in a chilled cutting solution
352 containing (in mM): 110 choline chloride, 25 NaHCO3, 25 D-glucose, 11.6 sodium ascorbate, 7 MgCl2,
353 3.1 sodium pyruvate, 2.5 KCl, 1.25 NaH2PO4, and 0.5 CaCl2 (Sigma Aldrich). Slices were then transferred
354 to artificial cerebrospinal fluid (ACSF) containing (in mM): 127 NaCl, 25 NaHCO3, 25 D-glucose, 2.5 KCl, 1
355 MgCl2, 2 CaCl2, and 1.25 NaH2PO4, aerated with 95% O2/5% CO2. Slices were first incubated at 34 °C
356 for 30 min and then maintained at room temperature for 20 min prior to use. Slices used for LSPS (1-2
357 per animal) contained barrels in the L4 of cortex, the globus pallidus, its external segment (GPe), the
358 internal capsule, the ventral posteromedial nucleus of thalamus and the anterior hippocampus. ~ 8
359 barrels (5-13) were visible in the slice. 2 rows of barrels may have been superimposed. At the end of
360 each experiment, a picture of the slice was saved in order to superimpose it digitally to other slices,
361 according to visual landmarks (Adobe Photoshop; Adobe Inc.). SPNs were visualized under infrared and
362 fluorescent lights in a BX61WI microscope (Olympus) and patched with borosilicate electrodes (3–6 MΩ)
363 and recorded in the voltage-clamp whole-cell configuration using a Multiclamp 700A amplifier (Axon
364 Instrument, Molecular Devices). The holding membrane potential was – 80 mV. The intracellular

365 solution contained (in mM) 128 Cs-methylsulfate, 4 MgCl2, 10 HEPES, 1 EGTA, 4 Na2ATP, 0.4 Na2GTP, 10
366 Na-phosphocreatine, 3 ascorbic acid; pH 7.25; 290-300 mOsm. Cells in L5 and L2/3 of the barrel cortex
367 were recorded in the current-clamp mode, with an intracellular solution in which Cs-methylsulfate was
368 replaced by K-methylsulfate. All experiments were performed at room temperature (21°C).

369 **LSPS with glutamate uncaging**

370 LSPS was performed as described previously (Bureau et al., 2006). Recirculating (2 mL/min) ACSF
371 solution contained (in mM): 0.2 MNI-caged glutamate (Tocris), 0.005 CPP [()-3-(2-carboxypiperazin-4-yl)
372 propyl-1-phosphonic acid], 4 $CaCl_2$, and 4 $MgCl_2$. Focal photolysis of caged glutamate was accomplished
373 with a 2 ms 20 mW pulse of a pulsed UV (355 nm) laser (DPSS Lasers Inc.) through a 0.16 NA 4 ×
374 objective (Olympus). 25 mW laser pulses were used for stimulating cortical neurons in mice older than
375 P30 to maintain their excitation at a similar level than in younger mice (Supplemental Fig. 2B). The
376 stimulus pattern for mapping the corticostriatal projections was 464 positions spaced by 75 µm on a 29
377 × 16 grid (2.1 × 1.1 mm) over barrel cortex. The corticostriatal slice and the LSPS grid were oriented in
378 such a way that layer 5a was laid out horizontally. UV stimuli were applied every 700 ms and their
379 successive positions on the LSPS grid were such as to maximize the time between stimulations of
380 neighboring sites. Electrophysiological traces consisted of 100 ms baseline, a 450 ms window followed
381 by a -5 mV 100 ms test pulse. A minimum of 2 and up to 4 stimulations were performed at each site at
382 several minutes intervals. Custom software for instrument control and acquisition (Suter et al. 2010)
383 was written in Matlab (Mathworks). Excitation profiles of pyramidal neurons were generated under
384 similar conditions except that cells were recorded in current-clamp mode and glutamate was uncaged
385 on a smaller 8 × 8 grid covering their soma and dendrites (50 µm spacing; 350 × 350 µm). In a subset of
386 L5a cell recordings, a 8 × 24 grid was used to stimulate up in L1 (50 µm spacing).

387 **Analysis of LSPS data**

388 Synaptic input maps of neurons were constructed by taking the peak amplitude of EPSCs detected in a
389 50 ms time window starting at stimulation onset for each position in the LSPS grid. Measures were
390 averaged across repetitions of stimulations (2-4). The threshold for EPSC detection was 3 standard
391 deviations from baseline, or 9.2 ± 0.4 pA. To disambiguate evoked responses from spontaneous activity,
392 synaptic responses occurring less than 2 times across repetitions of maps were set to zero. Averaged
393 maps were superimposed taking L5a as reference in the vertical axis and the junction of the GPe, dorsal
394 striatum and internal capsule as reference in the horizontal axis (Ref_{hor}). In order to detect connectivity
395 clusters and center of mass in the LSPS map, we used the binary version of the map ('connectivity map')

396 reporting the location of connected and non-connected sites (i.e., yielding EPSCs or none in the
397 recorded SPN). To detect clusters, the binary map was collapsed along its vertical axis. A cluster
398 comprised 1 or more consecutive connected sites that was framed by 1 or more non-connected sites.
399 Thus, a cluster here may include connected sites that were not adjacent on the vertical axis in the
400 original map, and may combine synaptic inputs from different layers. The number of cortical columns
401 was estimated based on the number of consecutive connected sites (ConsSites) in the collapsed map
402 and the mean width of a barrel in the slice, 150 µm, which is equal to 2 connected sites in the map.
403 Hence, the number of cortical columns = Σ (ceiling(ConsSites/2)). The connectivity center of mass was
404 computed based on the uncollapsed map as follows : Σ (Σ_{vert} connected sites × lateral distance from
405 Ref_{hor}) /Σ (Σ_{vert} connected sites). The synaptic input center of mass was computed based on the original
406 map, after thresholding, as follows: Σ ($mean_{vert}$ EPSC × lateral distance from Ref_{hor}) /Σ ($mean_{vert}$ EPSC).
407 Traces from current clamp recordings were analyzed to count the number of action potentials (APs)
408 elicited upon glutamate uncaging. In the 8 × 8 grid, 50 µm spacing, total number of spikes was 2.2 ± 0.2
409 for L2/3 pyramidal cells (n = 26), 5.4 ± 0.6 for regular spiking (RS) pyramidal cells in L5a (n = 30) and 9.9
410 ± 1.6 for non-RS pyramidal cells in L5b (n = 10). The number of spikes elicited by uncaging at single sites
411 was 1 or 2 and on average: 1.04 ± 0.04 for L2/3 cells, 1.03 ± 0.02 for L5 RS cells and 1.04 ± 0.02 for L5
412 non-RS cells. As spacing in the stimulation grid was 50 µm in these particular experiments, we used the
413 following equation to compute the number of sites with AP (sAP) in a stimulation grid with a spacing of
414 75 µm (i.e. as in connectivity maps): $sAP_{75} = sAP_{50} \times (75/50)^2$.

415 **Labeling of cortical cells**

416 In a somatosensory corticostriatal slice prepared as described above, biocytin (2 %) was injected by
417 iontophoresis in the L5a through a patch electrode (200 ms, 2.5 Hz) for 2 x 10 minutes (Chang, LoTurco
418 and Nisenbaum, 2000). The slice was incubated for 4 hours at room temperature in ACSF and
419 transferred to 4 % paraformaldehyde at 4°C overnight. It was rinsed in PBS containing 0.3 % Triton X-100
420 (PBS-T), incubated overnight at room temperature in streptavidin-AlexaFluor488 (1:1000 in PBS-T) and
421 mounted using Vectashield mount medium. Image acquisition was performed using a LSM 800 confocal
422 Zeiss microscope.

423 **Statistical analysis**

424 All data are expressed as mean ± SEM in the text. Median and 25-75th percentiles are shown in Figures.
425 N and n are the numbers of animals and neurons, respectively. Unless stated otherwise, paired or
426 unpaired non parametric tests, and Kruskal-Wallis test for repeated measures followed by Dunn post-

427 hoc test and Šidák correction for multiple comparisons were used. $p < 0.05$ is considered as statistically
428 significant.

429 **Acknowledgments:**

430 This work was supported by funding from the Institut National de la Santé et de la Recherche Médicale
431 and a grant from the Agence Nationale de la Recherche (Corticostriatal, ANR-20-CE16-0002). K.
432 Amroune is supported by fellowships from the Ministère de l'Enseignement Supérieur et de la
433 Recherche, from the governmental "France 2030" program via A*Midex (Initiative d'Excellence d'Aix-
434 Marseille Université, AMX-19-IET-004) and by ANR funding (ANR-17-EURE-0029). L. Fontolan is
435 supported by funding from Excellence Initiative of Aix Marseille Université - A*MIDEX (Turing Centre for
436 Living Systems). We thank the staff of the animal and genotyping facilities, the histology and imaging
437 platforms of INMED, the members of the CBGB group for their help and support and Elodie Fino, Rosa
438 Cossart, Ede Rancz, Roustem Khazipov, Thomas Morvan, Jean-Luc Gaiarsa, Corinne Beurrier and Lydia
439 Kerkerian Le Goff for their critical reading of the manuscript.

440 ## References

441 Ade KK, Wan Y, Chen M, Gloss B, Calakos N (2011) An Improved BAC Transgenic Fluorescent Reporter
442 Line for Sensitive and Specific Identification of Striatonigral Medium Spiny Neurons. Front Syst
443 Neurosci 5:32.

444 Adibi M (2019) Whisker-Mediated Touch System in Rodents: From Neuron to Behavior. Front. Syst.
445 Neurosci 13:40.

446 Alloway KD, Crist J, Mutic JJ, Roy SA (1999) Corticostriatal Projections from Rat Barrel Cortex Have an
447 Anisotropic Organization that Correlates with Vibrissal Whisking Behavior. J Neurosci 19:10908–
448 10922.

449 Alloway KD, Mutic JJ, Hoffer ZS, Hoover JE (2000) Overlapping corticostriatal projections from the rodent
450 vibrissal representations in primary and secondary somatosensory cortex. J Comp Neurol
451 428:51–67.

452 Aronoff R, Matyas F, Mateo C, Ciron C, Schneider B, Petersen CCH (2010) Long-range connectivity of
453 mouse primary somatosensory barrel cortex. Eur J Neurosci 31:2221–2233.

454 Ayaz A, Stäuble A, Hamada M, Wulf M-A, Saleem AB, Helmchen F (2019) Layer-specific integration of
455 locomotion and sensory information in mouse barrel cortex. Nat Commun 10:2585.

456 Benison AM, Ard TD, Crosby AM, Barth DS (2006) Temporal patterns of field potentials in vibrissa/barrel
457 cortex reveal stimulus orientation and shape. J Neurophysiol 95:2242–2251.

458 Bertero A, Verrillo L, Apicella AJ (2022) A Novel Layer 4 Corticofugal Cell Type/Projection Involved in
459 Thalamo-Cortico-Striatal Sensory Processing. J Neurosci 42:1383–1405.

460 Bertran-Gonzalez J, Bosch C, Maroteaux M, Matamales M, Hervé D, Valjent E, Girault J-A (2008)
461 Opposing patterns of signaling activation in dopamine D1 and D2 receptor-expressing striatal
462 neurons in response to cocaine and haloperidol. J Neurosci 28:5671–5685.

463 Braitenberg V, Schüz A (1998) Cortex: Statistics and Geometry of Neuronal Connectivity. Springer

464 Bureau I, Shepherd GMG, Svoboda K (2008) Circuit and plasticity defects in the developing
465 somatosensory cortex of FMR1 knock-out mice. J Neurosci 28:5178–5188.

466 Bureau I, von Saint Paul F, Svoboda K (2006) Interdigitated paralemniscal and lemniscal pathways in the
467 mouse barrel cortex. Plos Biol 4:e382

468 Cao J, Dorris DM, Meitzen J (2018) Electrophysiological properties of medium spiny neurons in the
469 nucleus accumbens core of prepubertal male and female Drd1a-tdTomato line 6 BAC transgenic
470 mice. J Neurophysiol 120:1712–1727.

471 Carelli RM, West MO (1991) Representation of the body by single neurons in the dorsolateral striatum of
472 the awake, unrestrained rat. J Comp Neurol 309:231–249.

473 Chang SL, LoTurco JJ and Nisenbaum LK (2000) In vitro biocytin injection into perinatal mouse brain: a
474 method for tract tracing in developing tissue. J Neurosci Methods 97:1-6

475 Cho J, West MO (1997) Distributions of single neurons related to body parts in the lateral striatum of the
476 rat. Brain Res 756:241–246.

477 Cowan RL, Wilson CJ (1994) Spontaneous firing patterns and axonal projections of single corticostriatal
478 neurons in the rat medial agranular cortex. J Neurophysiol 71:17–32.

479 Dash S, Autio DM, Crandall SR (2022) State-Dependent Modulation of Activity in Distinct Layer 6
480 Corticothalamic Neurons in Barrel Cortex of Awake Mice. J Neurosci 42:6551-6565

481 de la Torre-Martinez R, Ketzef M, Silberberg G (2023) Ongoing movement controls sensory integration in
482 the dorsolateral striatum. Nat Commun 14:1004.

483 Enoksson T, Bertran-Gonzalez J, Christie MJ (2012) Nucleus accumbens D2- and D1-receptor expressing
484 medium spiny neurons are selectively activated by morphine withdrawal and acute morphine,
485 respectively. Neuropharmacology 62:2463–2471.

486 Erlandson MA, Manzoni OJ, Bureau I (2015) The Functional Organization of Neocortical Networks
487 Investigated in Slices with Local Field Recordings and Laser Scanning Photostimulation. Plos One
488 10:e0132008.

489 Filipović M, Ketzef M, Reig R, Aertsen A, Silberberg G, Kumar A (2019) Direct pathway neurons in mouse
490 dorsolateral striatum in vivo receive stronger synaptic input than indirect pathway neurons. J
491 Neurophysiol 122:2294–2303.

492 Flaherty AW, Graybiel AM (1991) Corticostriatal transformations in the primate somatosensory system.
493 Projections from physiologically mapped body-part representations. J Neurophysiol 66:1249–
494 1263.

495 Flaherty AW, Graybiel AM (1994) Input-output organization of the sensorimotor striatum in the squirrel
496 monkey. J Neurosci 14:599–610.

497 Guo C, Peng J, Zhang Y, Li A, Li Y, Yuan J, Xu X, Ren M, Gong H, Chen S (2017) Single-axon level
498 morphological analysis of corticofugal projection neurons in mouse barrel field. Sci Rep 7:2846.

499 Hooks BM, Papale AE, Paletzki RF, Feroze MW, Eastwood BS, Couey JJ, Winnubst J, Chandrashekar J,
500 Gerfen CR (2018) Topographic precision in sensory and motor corticostriatal projections varies
501 across cell type and cortical area. Nat Commun 9:3549.

502 Jaeger D, Gilman S, Aldridge JW (1995) Neuronal activity in the striatum and pallidum of primates
503 related to the execution of externally cued reaching movements. Brain Res 694:111–127.

504 Kincaid AE, Zheng T, Wilson CJ (1998) Connectivity and Convergence of Single Corticostriatal Axons. J
505 Neurosci 18:4722.

506 Kravitz AV, Freeze BS, Parker PRL, Kay K, Thwin MT, Deisseroth K, Kreitzer AC (2010) Regulation of
507 parkinsonian motor behaviours by optogenetic control of basal ganglia circuitry. Nature
508 466:622–626.

509 Kress GJ, Yamawaki N, Wokosin DL, Wickersham IR, Shepherd GMG, Surmeier DJ (2013) Convergent
510 cortical innervation of striatal projection neurons. Nat Neurosci 16:665–667.

511 Kwon SE, Yang H, Minamisawa G, O'Connor DH (2016) Sensory and decision-related activity propagate in
512 a cortical feedback loop during touch perception. Nat Neurosci 19:1243–1249.

513 Mallet N, Le Moine C, Charpier S, Gonon F (2005) Feedforward inhibition of projection neurons by fast-
514 spiking GABA interneurons in the rat striatum in vivo. J Neurosci 25:3857–3869.

515 Oorschot DE (1996) Total number of neurons in the neostriatal, pallidal, subthalamic, and substantia
516 nigral nuclei of the rat basal ganglia: a stereological study using the cavalieri and optical disector
517 methods. J Comp Neurol 366:580–599.

518 Oryshchuk A, Sourmpis C, Weverbergh J, Asri R, Esmaeili V, Modirshanechi A, Gerstner W, Petersen CCH,
519 Crochet S (2024) Distributed and specific encoding of sensory, motor, and decision information
520 in the mouse neocortex during goal-directed behavior. Cell Rep 43:113618.

521 Parker PRL, Lalive AL, Kreitzer AC (2016) Pathway-Specific Remodeling of Thalamostriatal Synapses in
522 Parkinsonian Mice. Neuron 89:734–740.

523 Pennartz CMA, Berke JD, Graybiel AM, Ito R, Lansink CS, van der Meer M, Redish AD, Smith KS, Voorn P
524 (2009) Corticostriatal Interactions during Learning, Memory Processing, and Decision Making. J
525 Neurosci 29:12831–12838.

526 Peters A (1979) Thalamic input to the cerebral cortex. Trends Neurosci 2:183–185.

527 Pidoux M, Mahon S, Deniau J-M, Charpier S (2011) Integration and propagation of somatosensory
528 responses in the corticostriatal pathway: an intracellular study *in vivo*: Sensory responses in the
529 corticostriatal pathway. J Physiol 589:263–281.

530 Ramaswamy S, Markram H (2015) Anatomy and physiology of the thick-tufted layer 5 pyramidal neuron.
531 Front Cell Neurosci 9:233.

532 Reig R, Silberberg G (2014) Multisensory integration in the mouse striatum. Neuron 83:1200–1212.

533 Reiner A, Jiao Y, Del Mar N, Laverghetta AV, Lei WL (2003) Differential morphology of pyramidal tract-
534 type and intratelencephalically projecting-type corticostriatal neurons and their intrastriatal
535 terminals in rats. J Comp Neurol 457:420–440.

536 Shepherd GMG, Pologruto TA, Svoboda K (2003) Circuit analysis of experience-dependent plasticity in
537 the developing rat barrel cortex. Neuron 38:277–289.

538 Shepherd GMG, Svoboda K (2005) Laminar and columnar organization of ascending excitatory
539 projections to layer 2/3 pyramidal neurons in rat barrel cortex. J Neurosci 25:5670–5679.

540 Shepherd GMG, Stepanyants A, Bureau I, Chklovskii D, Svoboda K (2005) Geometric and functional
541 organization of cortical circuits. Nat Neurosci 8:782–790

542 Sippy T, Lapray D, Crochet S, Petersen CCH (2015) Cell-Type-Specific Sensorimotor Processing in Striatal
543 Projection Neurons during Goal-Directed Behavior. Neuron 88:298–305.

544 Smith Y, Bevan MD, Shink E, Bolam JP (1998) Microcircuitry of the direct and indirect pathways of the
545 basal ganglia. Neuroscience 86:353–387.

546 Thibault D, Loustalot F, Fortin GM, Bourque M-J, Trudeau L-É (2013) Evaluation of D1 and D2 Dopamine
547 Receptor Segregation in the Developing Striatum Using BAC Transgenic Mice. Plos One
548 8:e67219.

549 Vélez-Fort M, Rousseau CV, Niedworok CJ, Wickersham IR, Rancz EA, Brown APY, Strom M, Margrie TW
550 (2014) The stimulus selectivity and connectivity of layer six principal cells reveals cortical
551 microcircuits underlying visual processing. Neuron 83:1431-43

552 Wall NR, De La Parra M, Callaway EM, Kreitzer AC (2013) Differential innervation of direct- and indirect-
553 pathway striatal projection neurons. Neuron 79:347–360.

554 Wise SP, Jones EG (1977) Cells of origin and terminal distribution of descending projections of the rat
555 somatic sensory cortex. J Comp Neurol 175:129–157.

556 Wright AK, Norrie L, Ingham CA, Hutton EAM, Arbuthnott GW (1999) Double anterograde tracing of
557 outputs from adjacent “barrel columns” of rat somatosensory cortex. Neostriatal projection
558 patterns and terminal ultrastructure. Neuroscience 88:119–133.

559 Yamashita T, Vavladeli A, Pala A, Galan K, Crochet S, Petersen SSA, Petersen CCH (2018) Diverse Long-
560 Range Axonal Projections of Excitatory Layer 2/3 Neurons in Mouse Barrel Cortex. Front
561 Neuroanat 12:33.

562 Znamenskiy P, Zador AM (2013) Corticostriatal neurons in auditory cortex drive decisions during
563 auditory discrimination. Nature 497:482–485.

564

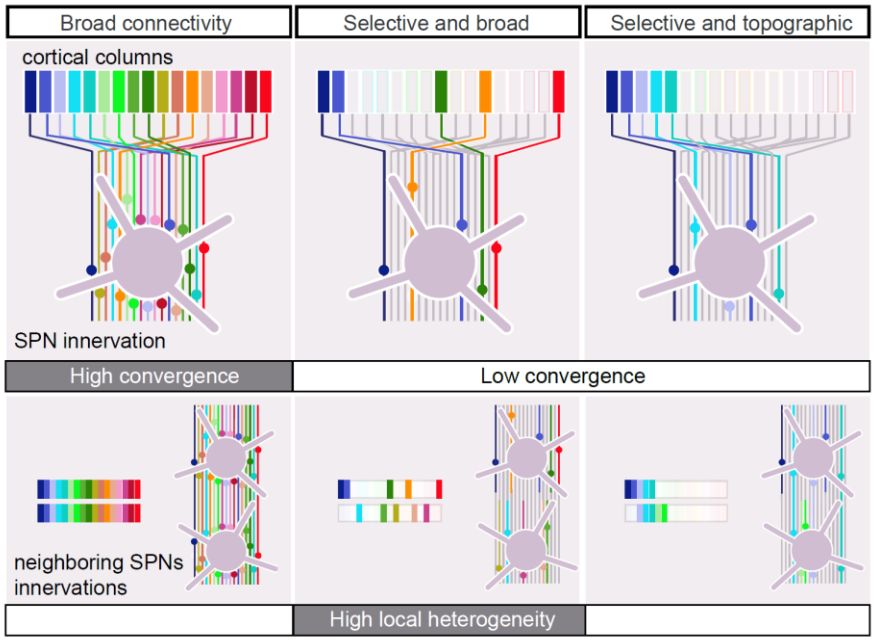

Figure 1. Potential connectivity patterns within the corticostriatal projection.
A rich and overlapping cortical innervation of the striatum (lines) permits different connectivity patterns: Left, synapses are formed promiscuously. In this case convergence is high as each SPN receives broad cortical input, from many cortical origins (colored bars on top). Middle and right, only a fraction of the potential connections are actually formed and, in these cases, convergence is lower. The selected presynaptic neurons are either scattered (middle) or topographically (right) positioned in the cortex. Increasing the selectivity of the corticostriatal connections while keeping their broad origin (middle) could generate maximal heterogeneity in the patterns of input for SPNs sharing the same striatal volume, due to a large number of combinations of cortical origins. In the case of a topographic innervation (right), neighboring SPNs form synapses with presynaptic neurons located in the same cortical region, reducing the local heterogeneity.

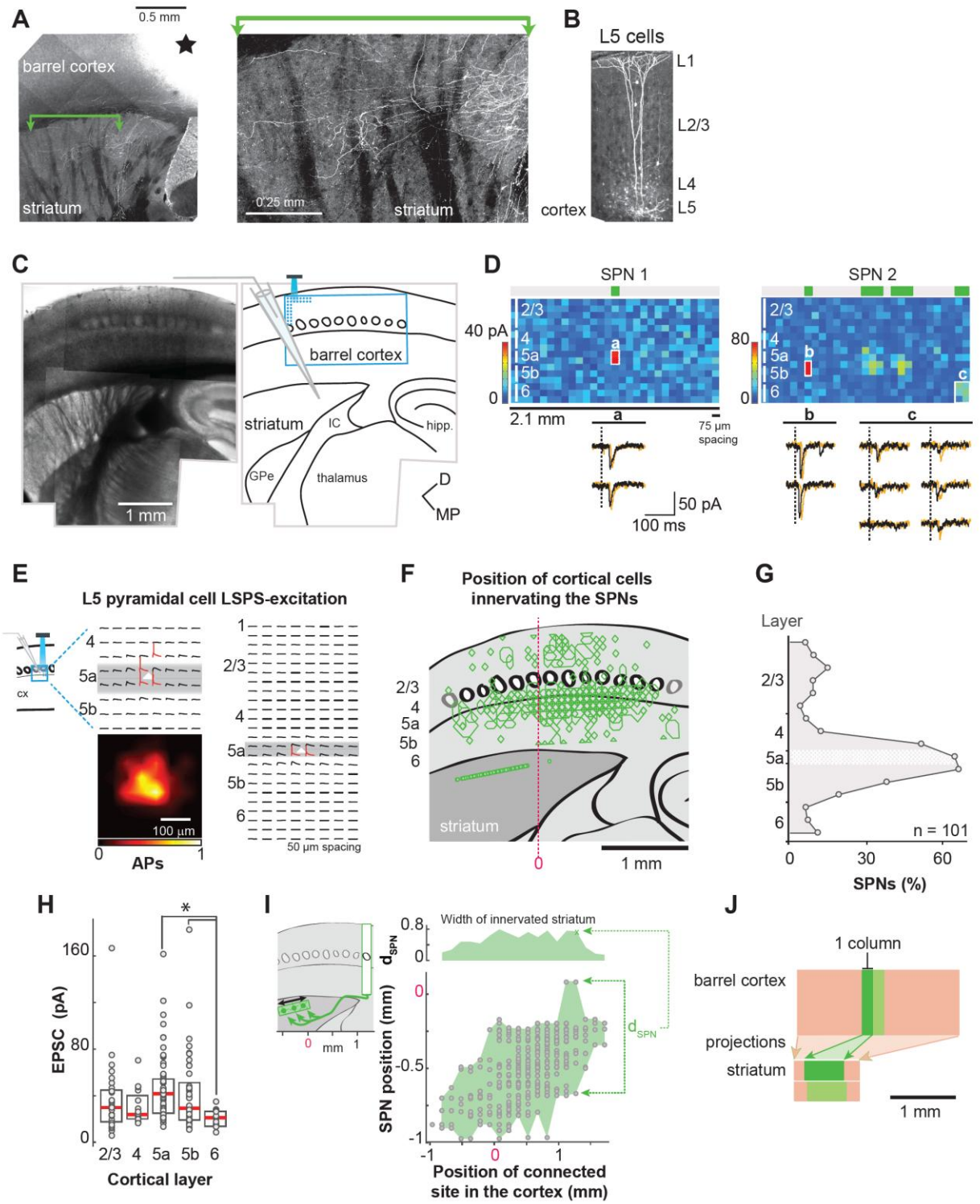

578

579 **Figure 2. A novel slice preparation for investigating the spatial organization of the somatosensory**
580 **projections to the DLS neurons.**
581 **A**. A somatosensory corticostriatal slice in which axons from L5 neurons were labeled with biocytin
582 iontophoresis. Black star, the electrode position in L5a. Right, focus on a region in the striatum.

583 **B.** Right, Example dendritic arbors of L5 cortical cells labeled with biocytin in the slice.
584 **C**. Montage of a corticostriatal slice (left) and layout of the experiment (right). A SPN was recorded in
585 the dorsolateral striatum while cortical neurons were photostimulated with LSPS. The grid of LSPS (blue)
586 was positioned on the barrel cortex. GPe, globus pallidus, external segment; IC, internal capsule; hipp.,
587 hippocampus.
588 **D**. Top, examples of synaptic input maps for individual SPNs showing one or four clusters of input (SPN 1
589 and 2, respectively). In the color maps, each pixel of color indicates the peak amplitude of EPSCs
590 detected within a 50 ms window after the stimulus onset. The different cortical layers are represented
591 by solid white vertical lines on the left side of the map. The green boxes at the top of the maps, the
592 clusters of sites in the connectivity maps collapsed in the vertical axis whose stimulation evokes EPSCs.
593 Bottom, EPSC traces evoked at the sites indicated by letters in the maps above. Two repetitions are
594 superimposed (black and orange). Vertical dashed lines, the stimulus onsets (2 ms stimulus).
595 **E.** LSPS evoked excitation of two L5a pyramidal neurons recorded in current-clamp mode. LSPS was a 8 x
596 8 (left) or 24 x 8 (right) 50 µm spacing grid. Cortical neurons are positioned at the center (white
597 triangles). Traces with an action potential are in red. Bottom, Average number of action potentials
598 evoked at every site of the LSPS grid.
599 **F**. Overlay of the sites in the barrel cortex (green polygons) where stimulations evoked EPSCs in SPNs
600 (green symbols; n =101 cells, N = 54 mice). The red dashed vertical line is the reference (Ref_{hor} in the
601 Methods) used for aligning slices across experiments horizontally.
602 **G**. Contribution of each cortical layer to the SPN innervations. The 16 rows of the grid correspond to
603 different cortical layers (Layer 2/3: 1-6; L4: 7-9; L5a: 10; L5b: 11-13; L6: 14-16). The horizontal white
604 band is L5a.
605 **H.** Amplitude of SPN EPSCs as a function of their laminar origin. Median (red) and 25-75th percentiles
606 (boxes). * Kruskal-Wallis p = 0.000125, Dunn-Šidák posthoc tests, p = 0.0001 and 0.03415.
607 **I.** Bottom, Positions of SPNs in the striatum for each position of connected sites on the horizontal axis of
608 the LSPS grid. Top, maximal distance between SPNs (d_{SPN}) for every connected site position in the barrel
609 cortex on the horizontal axis, binned every 150 µm, in other words the width of the projection zone of
610 one cortical column within the striatum
611 **J**. Schematic of the slice with the size of the cortical and striatal regions that are connected by
612 projections to SPNs (pink) and the size of the striatal domain with functional projections from a single
613 cortical column (shades of green).
614

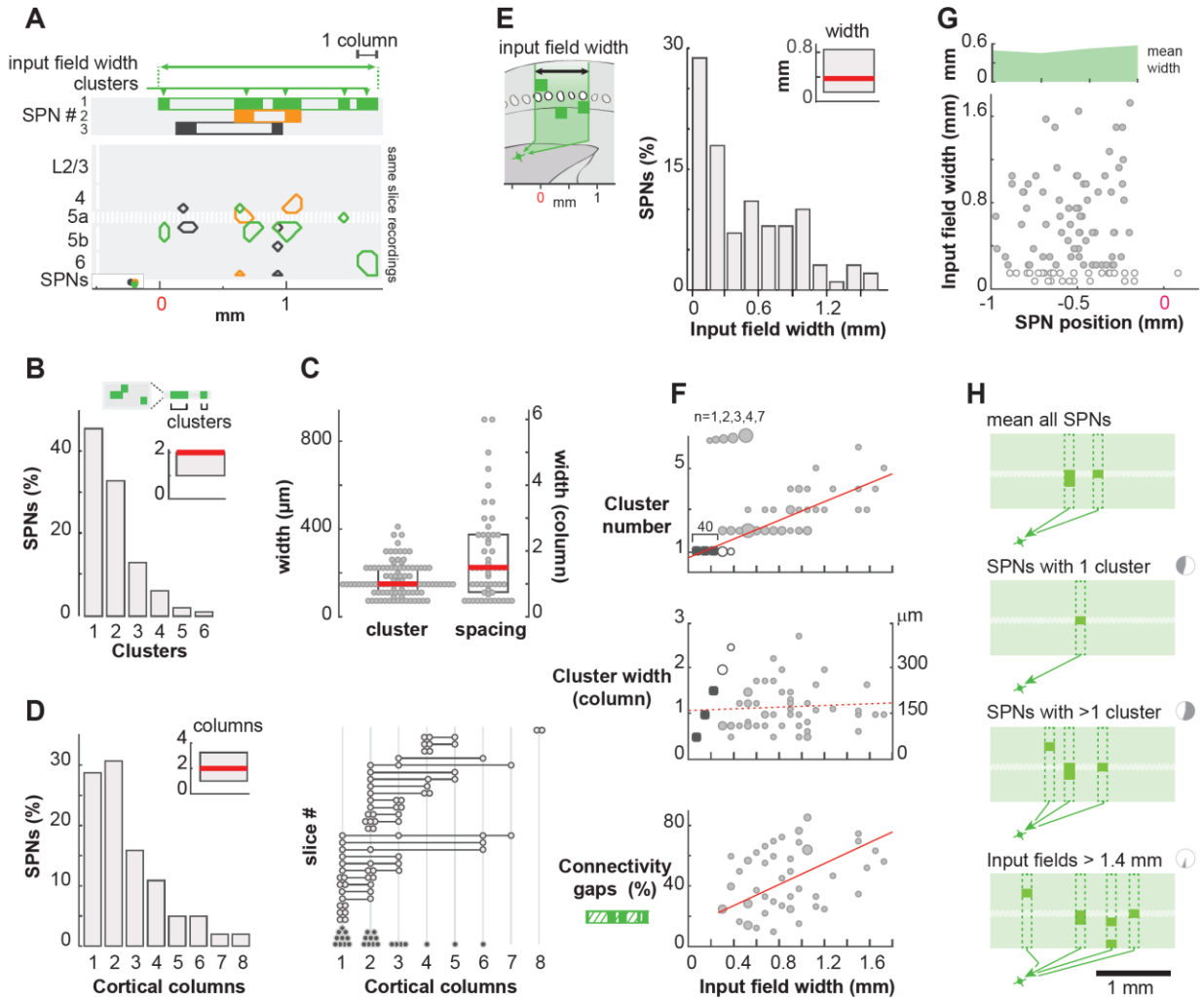

Figure 3. Sparse functional projections from the barrel cortex to individual SPNs in the DLS.

A. Example slice with 3 recordings. The hatched horizontal band is L5a, the polygons are the stimulation sites evoking EPSCs, the solid boxes on top are the connectivity clusters and the open rectangle the input field in the collapsed connectivity map. The circles at the bottom mark the positions of SPNs on the horizontal axis. Recordings are color coded.

B. Fraction of SPNs receiving inputs from 1 to 6 clusters of projections in the barrel cortex. In inset, median (red) and 25-75th percentiles (box). Clusters are defined as the ensemble of contiguous sites in the connectivity map collapsed in the vertical axis, whose stimulation evokes EPSCs (see examples in A, boxes at the top). n = 101 cells, N = 54 mice.

C. Median (red) and 25-75th percentiles (box) of cluster width and spacing.

D. Left, Fraction of cells receiving inputs from 1 to 8 cortical columns in the barrel area. In inset, median (red) and 25-75th percentiles (box). Right, Number of cortical columns innervating individual SPNs. Symbols are cells, lines are slices. Light gray symbols, slices with ≥ 2 recordings. Dark symbols, one recording per slice.

E. Fraction of SPNs with input fields from 0.075 to 1.6 mm.

F. Top to bottom, For every input field width, the number of clusters, cluster width (expressed in cortical column and µm) and proportion of connectivity gap, in input fields collapsed along the vertical axis. Gray symbols, cells with ≥ 2 connectivity clusters. Other symbols, cells with 1 cluster.
G. Bottom, width of input fields in the barrel cortex for different positions of SPNs in the striatum. SPNs with an input field the size of a single or of several cortical columns are shown (open and solid symbols, respectively). Top, The average width of input fields as a function of SPN positions binned every 250 µm.
H. Schematized average and principal connectivity patterns. In pie charts, the SPN proportions.

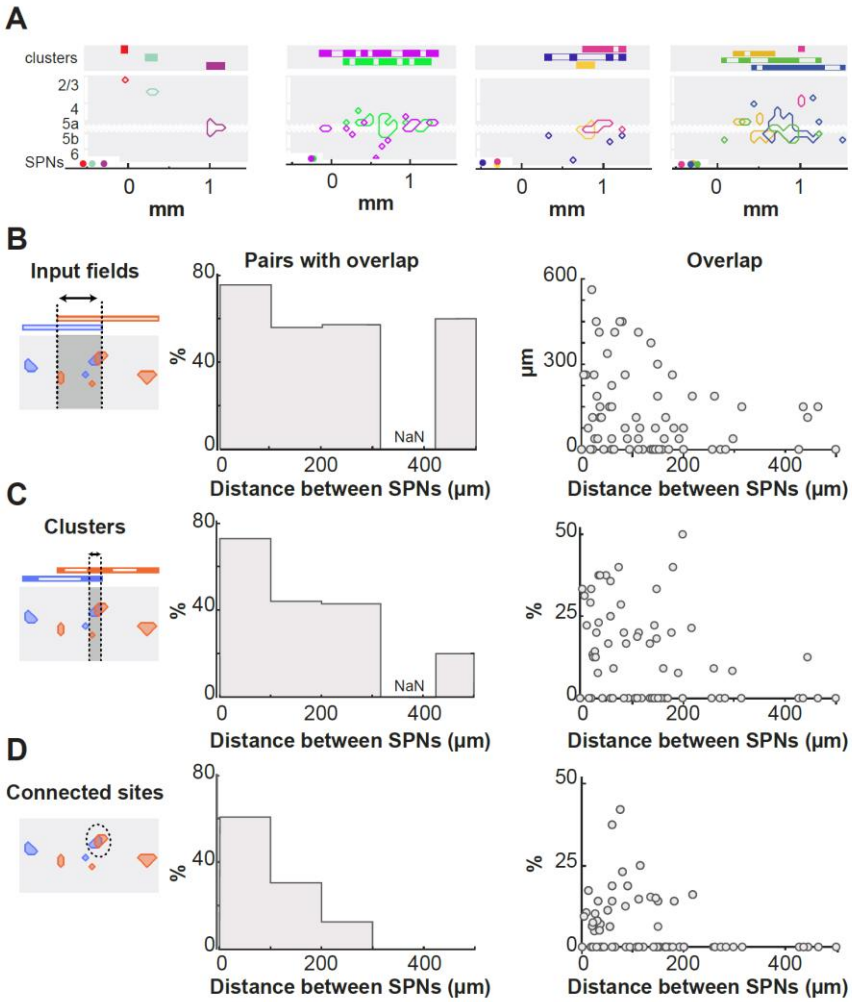

Figure 4. Individual SPNs have unique cortical innervation
A. Four example slices with 2 to 4 recordings. Same as in Fig. 2A.
B. Left, fraction of pairs with overlap in their input field. Right, width of overlap as a function of the horizontal distance separating cells. n = 70 pairs.
C. Same as in B for the fraction of vertical alignment between SPN connectivity maps.
D. Same as in B for the fraction of overlap between SPN connectivity maps.

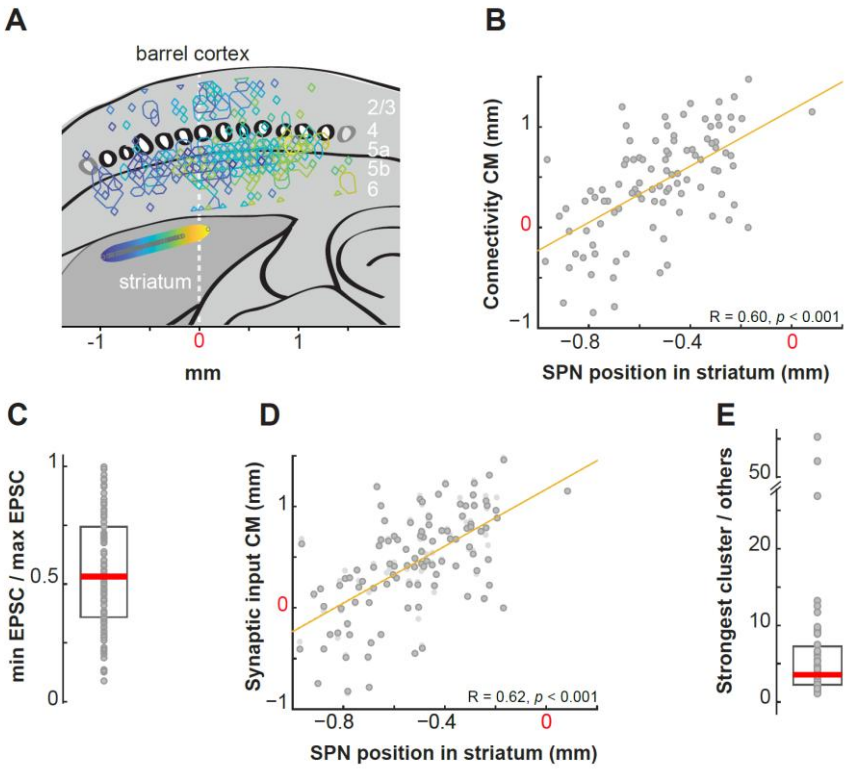

Figure 5. Topographic organization of the functional vibrissal innervation of SPNs in the DLS

A. Overlay of the sites in the barrel cortex where stimulations evoked EPSCs in SPNs. The colors, yellow to blue, indicate the position of the SPNs (gray circles) along the horizontal axis in the striatum (axis at the bottom, 0 is Ref_{hor} in the Methods; n = 101, N = 54). Blue shades are for lateral SPNs.

B. Position of the connectivity center of mass (CM) as a function of the SPN position in dorsal striatum. Zero on the x and y axis is the position of the vertical dashed line shown in A.

C. Ratio of the largest EPSC over the smallest EPSC for each recording. Median (red) and 25-75th percentiles (box).

D. Position of the synaptic input CM as a function of the SPN position in dorsal striatum. In light gray, the connectivity CM.

E. EPSC sum obtained in the strongest connectivity cluster relative to others sum. Cells with ≥ 2 clusters, n = 55.

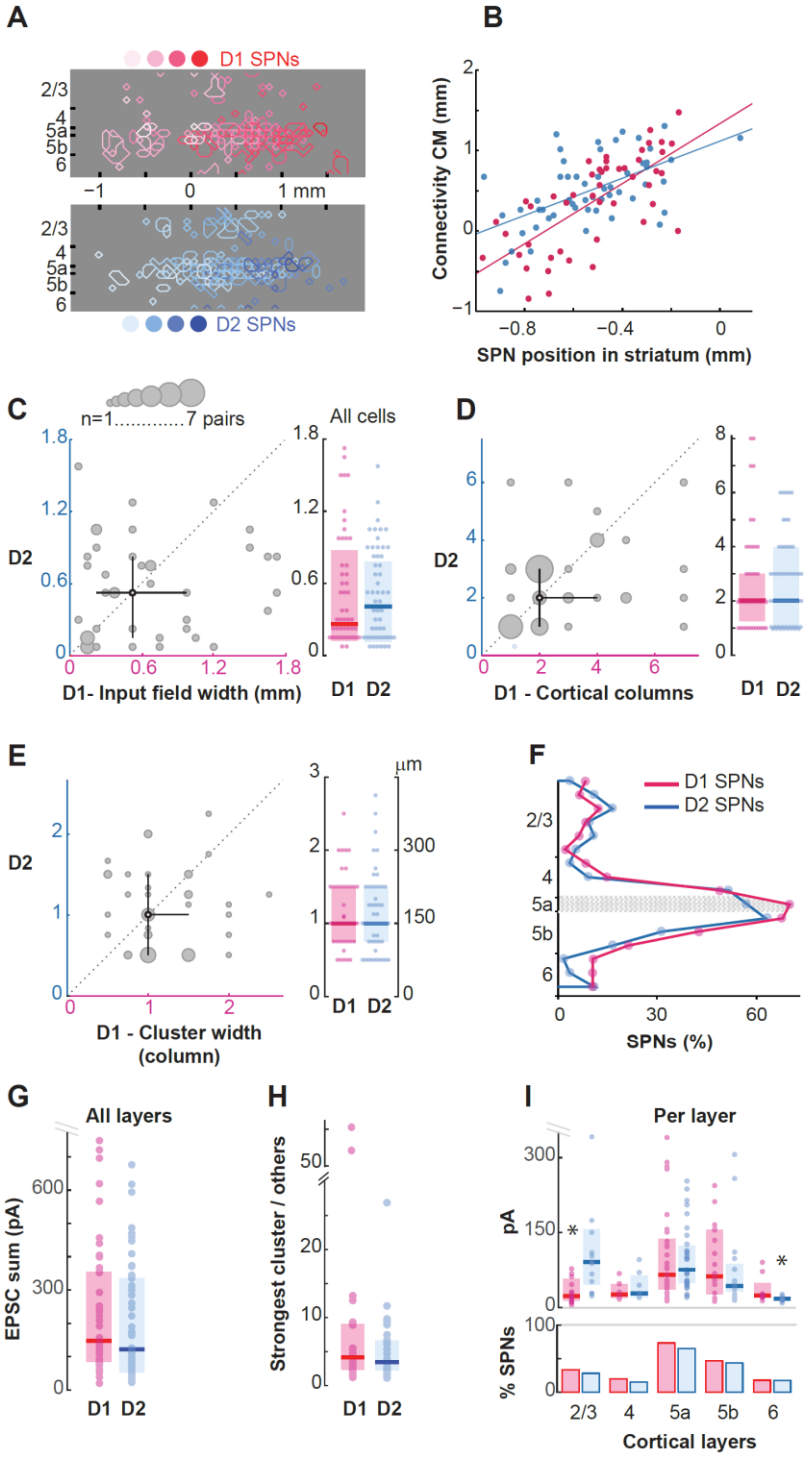

Figure 6. D1 and D2 SPNs have similar patterns of innervation from the barrel cortex

A. Overlay of the sites in the barrel cortex where stimulations evoked EPSCs in D1 (blue) or D2 SPNs (red). The shades, light to dark, indicate the position of the SPNs (bottom circles) along the medio-lateral axis in the dorsal striatum (axis at the bottom). D1 cells, n = 47, N = 36; D2 cells, n = 54, N = 37.

B. Position of the connectivity center of mass (CM) as a function of the SPN position in the dorsal striatum (D1, red; D2, blue). R = 0.70 (D1, n = 47, N = 36); R = 0.57 (D2, n = 54, N = 37).

C. Left, D2 SPN input field width as a function of the D1 SPN input field width, in the same slice. The black symbol and lines are the median value and 25-75th percentiles. Large symbols indicate n = 2 to 3 pairs. n = 42 pairs. Right, medians (thick lines) and 25-75th percentiles (boxes) of D1 and D2 input field widths, across all cells. n = 101.

D. Same as in C for the number of cortical columns.

E. Same as in C for the width of connectivity clusters.

F. Contribution of each cortical layer to the SPN innervations. The horizontal hatched band is L5a.

G. EPSC sum for D1 and D2 SPNs. Outliers were not shown for clarity (1 D1, 2 D2, 1.2-1.5 nA)

H. EPSC sum obtained from the strongest cluster relative to others. Cells with ≥ 2 clusters. D1, n = 24; D2, n = 30.

I. Top, D1 and D2 SPN EPSC sum as a function of laminar origin. For each layer, only cells with inputs are included. Outliers are not shown for clarity (3 D1, 2 D2, 350-700 pA). * indicates a significant difference (p = 0.005 and p = 0.008; Mann-Whitney). Bottom, fraction of cells with input.

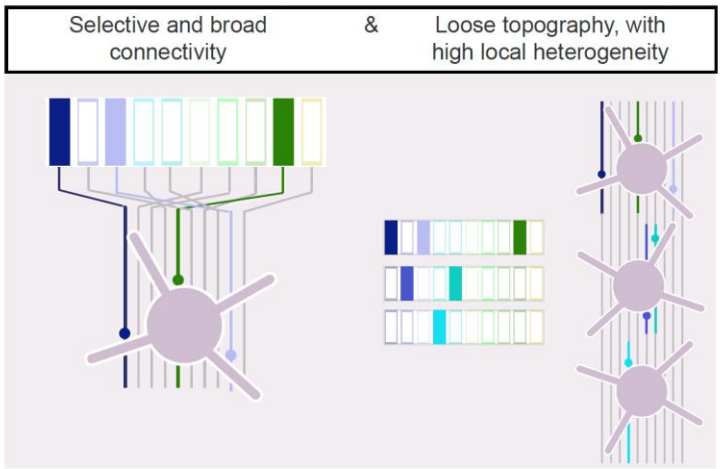

Figure 7. Connectivity pattern within the somatosensory corticostriatal projection to SPNs. Left, Our results support the model in which each SPN integrates limited and heterogeneous rather than exhaustive inputs transmitted by the barrel cortex, intermediate between the middle and right panels in Fig. 1. Right, Each SPN representation of the whisker cortical columns complements the representations of its neighbors.

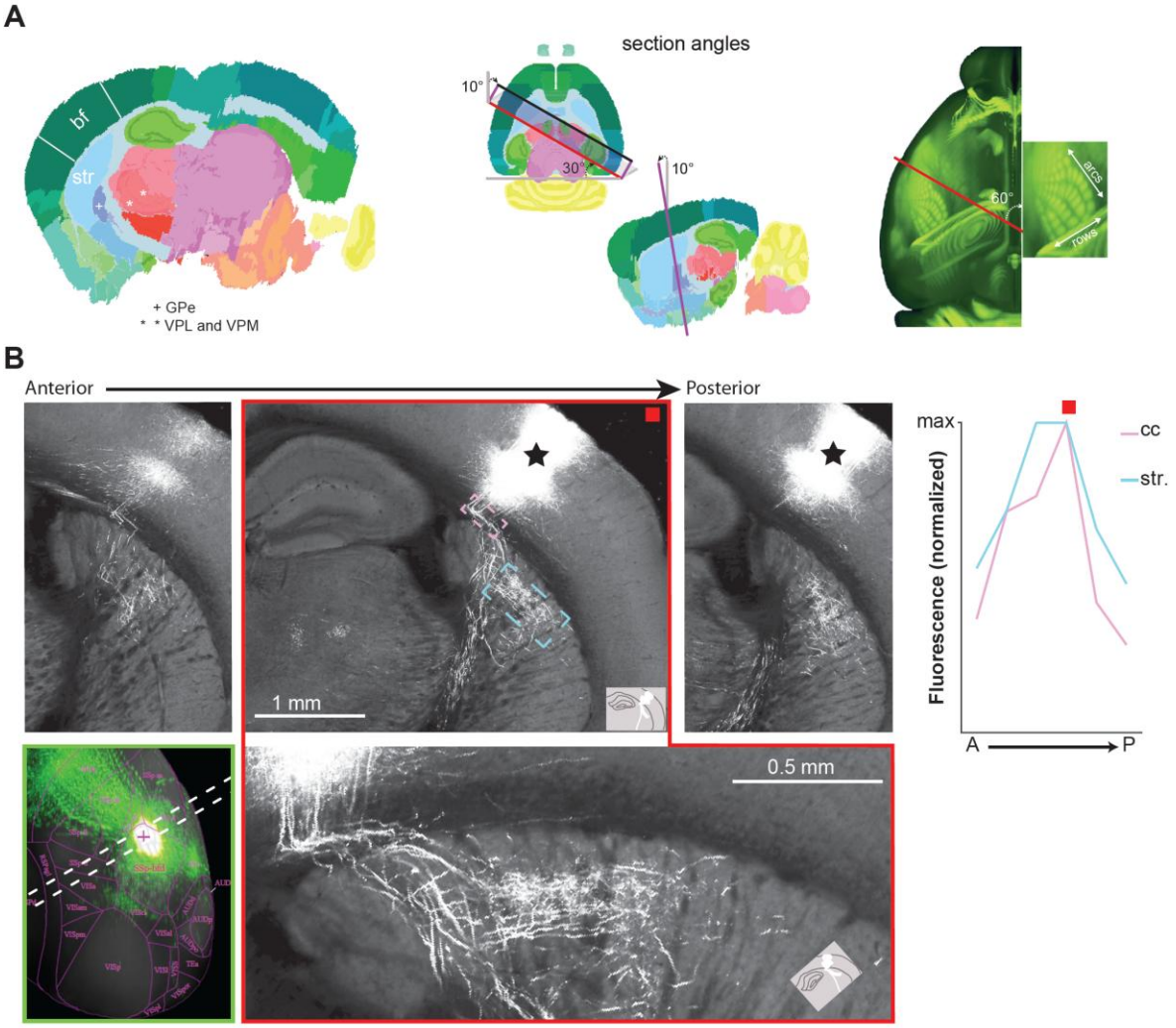

Supplemental Figure 1.

A. Left, the corticostriatal slice generated from the Allen mouse brain reference atlas (CutNII custom-angle slice visualization tool; G. Csucs). bf, barrel field. str, striatum. VPL, ventral posterolateral thalamic nucleus. VPM, ventral posteromedial thalamic nucleus. Center, the section angles illustrated on horizontal and longitudinal sections of the brain. Right, the section angle with respect to the orientations of the arcs and rows in the barrel field of the left hemisphere (Allen mouse brain atlas).

B. A simulated somatosensory corticostriatal slice generated using data from the Allen mouse connectivity atlas (https://connectivity.brain-map.org/projection/experiment/cortical_mp/293728197). eGFP was expressed in L2/3 and L5 pyramidal cells principally, in 3-4 arcs of the D and E rows of whisker columns (whole brain visualization in the green box at the bottom left; the dashed lines indicate the slice orientation). Acquisitions of serial two-photon tomography were stacked in Fiji and the reconstituted brain was sectioned using the angles to produce the acute somatosensory corticostriatal slices (BigDataViewer plugging). The red box identifies the "experimental slice" with intact projections from the barrel cortex to the striatum. Fluorescence in the striatum (blue) and in the corpus callosum (cc, pink) was quantified on consecutive max projections (300 µm thick) obtained in the anterior-posterior

703 axis (A-P). Note that slices, being from the opposite hemisphere to our experiments, have the reverse
704 orientation in the medio-lateral axis compared to Fig. 2A,C.
705
706

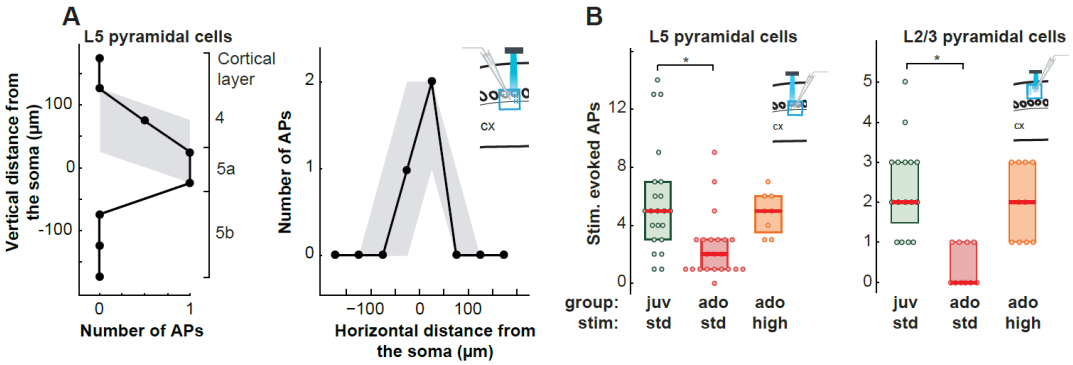

707

708 **Supplemental Figure 2.**
709 **A**. Vertical (left) and horizontal (right) excitation profile of L5 pyramidal cells recorded in current clamp,
710 in the juveniles and adolescents combined (20 and 25 mW stimulation, respectively). Evoked action
711 potentials (APs) were summed along each column (left) or line (right) of the LSPS grid (50 µm spacing).
712 Solid line, median. In gray, 25-75th percentiles. n = 30, N = 14.
713 **B.** Total number of APs evoked in the stimulation grid for L5 (left) and L2/3 (right) pyramidal cells in
714 juvenile (juv, P22-30) and adolescent (ado, P31-41) mice. A higher stimulation intensity was used for
715 adolescent mice (25 mW instead of the standard -std - intensity, 20 mW), so that the total number of
716 APs matched between the two age groups. L5, juv, n = 22, N = 9 ; ado std, n = 22, N = 13; ado high: n = 8,
717 N = 5; L2/3, juv: n = 16, N=3; ado std and high n = 10, N = 2; * $p < 0.001$, Mann-Whitney.
718